Structured emission of tetrahedral complexes due to Jahn-Teller and pseudo-Jahn-Teller effects

M. Bacci and S. Porcinai
Istituto di Ricerca sulle Onde Elettromagnetiche del Consiglio Nazionale delle Ricerche, Via Panciatichi 64, 50 127 Firenze, Italy

E. Mihóková, M. Nikl, and K. Polák
Institute of Physics, Academy of Sciences of the Czech Republic, Cukrovarnická 10, 162 53 Prague 6, Czech Republic
(Received 4 January 2001; revised manuscript received 18 April 2001; published 22 August 2001)

Tetrahedral complexes with an excited state consisting of two closely lying triplet states are considered. The full interaction Hamiltonian, including ligand field, Jahn-Teller, pseudo-Jahn-Teller, and spin-orbit interactions is constructed. The emission-band shape is numerically calculated within the semiclassical approach using Monte Carlo integration. The results of this numerical analysis are applied to the $PbWO_4$ system. Comparison with experimentally obtained spectra shows that this theory explains the observed triple-peak structure.

DOI: 10.1103/PhysRevB.64.104302 PACS number(s): 63.20.Kr, 71.70.−d, 78.55.Hx, 79.90.+b

I. INTRODUCTION

Closed-shell transition-metal ions of the type $(MO_4)^{q-}$ (M=V, Cr, Mo, W, Mn; $q=1-3$), have been extensively studied both from the experimental and theoretical points of view.[1] Ballhausen first demonstrated[2] that the promotion of a t_1 electron to an e orbital in such tetrahedral systems produced a set of four low-lying excited states, $^1T_2$, $^1T_1$, $^3T_1$, and $^3T_2$. The two spin triplets are at the lowest energy and are expected to be very close to each other in energy. Such a level scheme seems to be suitable for luminescence processes, and recent experiments[3,4] have confirmed luminescence even for the $(CrO_4)^{2-}$ ion, which for a long time appeared to be a nonluminescent system. By contrast, the luminescence arising from $(WO_4)^{2-}$ ions has been well known for a long time.[5] In particular, optical and luminescence characteristics of lead tungstate [$PbWO_4$ (PWO)] were first reported in the 1940s,[6] while more detailed studies of its luminescent centers appeared later.[7,8] Essentially two emission components were resolved. The so-called blue component, peaking around 420 nm, is based on radiative deexcitation of the regular oxyanion group $(WO_4)^{2-}$, while the defect-based green emission component is ascribed to a radiative transition in the oxygen-deficient oxyanion group WO_3. Renewed interest in the PWO single crystal arose several years ago due to its favorable scintillation characteristics, as a result of which it was selected for use in the construction of an electromagnetic calorimeter—the inner part of detecting systems[9,10]—in the large hadron collider that is being built in CERN. In this way PWO crystals have become very important for contemporary high-energy-physics measurements. Detailed reports dealing with PWO luminescence and scintillation characteristics have been published, and the nature and role of various defect states in the processes of energy transfer and storage has become a subject of debate (for a review see Ref. 11). Among other features, the rather peculiar shape of the blue-component emission spectrum was noticed.[12] It consists of a clearly resolved central peak and two side wings. A similar spectral shape was also reported[13] for other scheelite tungstates ($CaWO_4$, $BaWO_4$, $SrWO_4$). The lowest excited state of the tungstates is dominated by molecular orbitals associated with a $(WO_4)^{2-}$ group.[14] A possible role of the Jahn-Teller (JT) effect that can modify the $(WO_4)^{2-}$ tetrahedron was offered to explain the particular structure of the spectra. Consideration of the JT effect provided a similar triplet structure for the calculated emission band shape for the $^3T_{1u}\rightarrow{}^1A_{1g}$ transition in systems with O_h symmetry.[15] Similar structured emission was also obtained quantum mechanically.[16] However, the occurrence of two closely lying degenerate levels and the interplay of JT, pseudo Jahn-Teller (PJT), and spin-orbit (SO) interactions in the tetrahedral systems under consideration can give rise to adiabatic potential-energy surfaces (APES's) that cannot easily be understood without a complete numerical analysis. That, of course, is also reflected in the emission characteristics (intensity, band shape, decay time) of crystals containing $(MO_4)^{q-}$ units.

Accordingly, in the present work we perform a general theoretical analysis of tetrahedral complexes in which the lowest excited state consists of two closely lying triplet levels, and we also calculate the resulting emission spectra. The full interaction Hamiltonian of the problem includes ligand field (LF), JT, PJT, and SO interactions. The emission spectra of the system are numerically calculated within the semiclassical approach of Toyozawa and Inoue[17] by using a Monte Carlo technique to perform numerical integration. The calculated spectra are then qualitatively compared to the experimentally obtained emission band shape of PWO.

II. THEORY

A. Hamiltonian of the problem

According to molecular-orbital calculations,[2,14] the ground state $^1A_1$ of the closed-shell ions $(MO_4)^{q-}$ in T_d symmetry derives from the one-electron configuration $t_1^6e^0$. The first excited states are obtained by promoting one t_1 electron to the e levels. The resulting electronic configuration, $t_1^5e^1$, yields a set of four electronic states, $^1T_2$, $^1T_1$, $^3T_1$, and $^3T_2$. The energy gap Δ between the two latter states is expected to be very small, because to a first approximation[2] the only difference is due to Coulomb integrals involving $2p$ oxygen orbitals. Because both these levels are orbitally degenerate, they are JT unstable with respect

to the tetragonal (ϵ) and trigonal (τ_2) vibrational modes.[18] Furthermore, taking into account the direct product $t_1 \times t_2 = a_1 + e + t_1 + t_2$ and the smallness of the energy gap Δ, the PJT interaction between the two levels cannot be omitted. Finally, SO coupling has to be included, particularly when heavy atoms, like Mo or W, are present. Consequently, the total Hamiltonian of the problem we consider is given by

$$H_{\mathrm{TOT}} = H_{\mathrm{LF}} + H_{\mathrm{JT}} + H_{\mathrm{PJT}} + H_{\mathrm{SO}}, \tag{1}$$

where H_{LF}, H_{JT}, H_{PJT}, and H_{SO} are ligand field, JT interaction, PJT interaction, and SO coupling, respectively. We chose X, Y, Z and ξ, η, ζ as the orbital base functions for the ${}^3T_1$ and ${}^3T_2$ states, respectively, and S_x, S_y, S_z as the triplet spin functions. The total spin-orbital problem leads to an 18×18 Hamiltonian matrix with the basis functions

$$\begin{aligned} {}^3T_1: &\quad |XS_i\rangle, \quad |YS_i\rangle, \quad |ZS_i\rangle, \\ {}^3T_2: &\quad |\xi S_i\rangle, \quad |\eta S_i\rangle, \quad |\zeta S_i\rangle, \quad i = x,y,z. \end{aligned} \tag{2}$$

The full Hamiltonian matrix written in this basis is

$$H = \begin{pmatrix} H_{11} + \Delta \mathcal{I} & H_{12} \\ H_{21} & H_{22} \end{pmatrix}, \tag{3}$$

where H_{ij} $(i,j = 1,2)$ are 9×9 blocks and $\mathcal{I}$ is the 9×9 unit matrix. If we assume, for simplicity, that the coupling to the vibrational modes within the ${}^3T_1$ and ${}^3T_2$ levels is the same, then the diagonal blocks of the Hamiltonian (3) are equal ($H_{11} = H_{22}$) and are given by

$$H_{11} = \begin{pmatrix} & & & 0 & -\lambda & 0 & 0 & 0 & -\lambda \\ & H_{\mathrm{el}} & & \lambda & 0 & 0 & 0 & 0 & 0 \\ & & & 0 & 0 & 0 & \lambda & 0 & 0 \\ 0 & \lambda & 0 & & & & 0 & 0 & 0 \\ -\lambda & 0 & 0 & & H_{\mathrm{el}} & & 0 & 0 & -\lambda \\ 0 & 0 & 0 & & & & 0 & \lambda & 0 \\ 0 & 0 & \lambda & 0 & 0 & 0 & & & \\ 0 & 0 & 0 & 0 & 0 & \lambda & & H_{\mathrm{el}} & \\ -\lambda & 0 & 0 & 0 & -\lambda & 0 & & & \end{pmatrix}. \tag{4}$$

The SO interaction is evaluated by means of the Hamiltonian

$$H_{\mathrm{SO}} = \sum_i \sigma_i \mathbf{l_i} \cdot \mathbf{s_i}, \tag{5}$$

where σ_i is the single-electron SO coupling. If we assume that all the electrons involved are equivalent, so that $\sigma_i = \sigma$ for each i, the matrix elements in Eq. (4) are obtained by putting $\lambda = -\sigma/4$. This yields the single SO blocks (${}^3T_1$ and ${}^3T_2$), written as is usually found in the literature.[19] H_{el} in Eq. (4) is a part of the electron-lattice Hamiltonian that includes the JT interaction and the potential energy of the lattice (see, e.g., Ref. 20),

$$\begin{aligned} H_{\mathrm{el}} = &\begin{pmatrix} aQ_1 + b(Q_2 - Q_3/\sqrt{3}) & cQ_6 & cQ_5 \\ cQ_6 & aQ_1 - b(Q_2 + Q_3/\sqrt{3}) & cQ_4 \\ cQ_5 & cQ_4 & aQ_1 + 2bQ_3/\sqrt{3} \end{pmatrix} \\ &+ \left\{ \frac{1}{2} K_\alpha Q_1^2 + \frac{1}{2} K_\epsilon (Q_2^2 + Q_3^2) + \frac{1}{2} K_\tau (Q_4^2 + Q_5^2 + Q_6^2) + W_0 \right\} \mathcal{J}. \end{aligned} \tag{6}$$

In Eq. (6), Q_i are the symmetry coordinates, transforming as α (Q_1), ϵ $(Q_2 = Q_\epsilon,\ Q_3 = Q_\theta)$, and τ_2 $(Q_4 = Q_\xi,\ Q_5 = Q_\eta,\ Q_6 = Q_\zeta)$; a, b, and c are the linear electron-lattice coupling parameters, the K's are the elastic constants, W_0 is the energy of the ${}^3T_2$ state, and $\mathcal{J}$ is the tridimensional unit matrix.

The off-diagonal blocks of Eq. (3), $H_{12} = H_{21}$, are the following:

$$H_{12} = \begin{pmatrix} B_{1,10} & C_{1,11} & C_{1,12} & 0 & \sqrt{3}\lambda & 0 & 0 & 0 & -\sqrt{3}\lambda \\ -C_{1,11} & B_{2,11} & C_{1,13} & \sqrt{3}\lambda & 0 & 0 & 0 & 0 & 0 \\ -C_{1,12} & -C_{1,13} & B_{3,12} & 0 & 0 & 0 & -\sqrt{3}\lambda & 0 & 0 \\ 0 & -\sqrt{3}\lambda & 0 & B_{1,10} & C_{1,11} & C_{1,12} & 0 & 0 & 0 \\ -\sqrt{3}\lambda & 0 & 0 & -C_{1,11} & B_{2,11} & C_{1,13} & 0 & 0 & \sqrt{3}\lambda \\ 0 & 0 & 0 & -C_{1,12} & -C_{1,13} & B_{3,12} & 0 & \sqrt{3}\lambda & 0 \\ 0 & 0 & \sqrt{3}\lambda & 0 & 0 & 0 & B_{1,10} & C_{1,11} & C_{1,12} \\ 0 & 0 & 0 & 0 & 0 & -\sqrt{3}\lambda & -C_{1,11} & B_{2,11} & C_{1,13} \\ \sqrt{3}\lambda & 0 & 0 & 0 & -\sqrt{3}\lambda & 0 & -C_{1,12} & -C_{1,13} & B_{3,12} \end{pmatrix}. \tag{7}$$

The meaning of the matrix elements is as follows:

$$B_{1,10}=-b_{12}[(Q_2/2)+(\sqrt{3}Q_3/2)],$$
$$B_{2,11}=-b_{12}[(Q_2/2)-(\sqrt{3}Q_3/2)],$$
$$B_{3,12}=b_{12}Q_2 \quad C_{1,11}=-c_{12}Q_6, \tag{8}$$
$$C_{1,12}=c_{12}Q_5 \quad C_{1,13}=-c_{12}Q_4,$$

where b_{12} and c_{12} are PJT coupling parameters, related to ϵ and τ_2, respectively.

B. Emission band shape

According to the classical Franck-Condon approximation, the normalized line-shape function of the optical emission ${}^3T_{1,2}\rightarrow A_1$ may be written in a similar way as in Refs. 21 and 22 if a thermal distribution around the coordinates $(Q_1^0,Q_2^0,\ldots,Q_6^0)$ of the minimum on the excited-state APES is assumed:[15]

$$\begin{aligned} f(E)=&\left(\frac{K_\alpha}{2\pi k_BT}\right)^{1/2}\left(\frac{K_\epsilon}{2\pi k_BT}\right)\left(\frac{K_\tau}{2\pi k_BT}\right)^{3/2}\\ &\times\sum_i^6\int\cdots\int dQ_1dQ_2\cdots dQ_6|\langle g_j|\mathbf{M}|e_i\rangle|^2\\ &\times\exp\Bigg[-\frac{K_\alpha}{2k_BT}(Q_1-Q_1^0)^2-\frac{K_\epsilon}{2k_BT}\{(Q_2-Q_2^0)^2\\ &+(Q_3-Q_3^0)^2\}-\frac{K_\tau}{2k_BT}\{(Q_4-Q_4^0)^2+(Q_5-Q_5^0)^2\\ &+(Q_6-Q_6^0)^2\}\Bigg]\delta(E-X_{ij}(Q_1,Q_2,\ldots,Q_6)), \end{aligned} \tag{9}$$

where E is the photon energy, k_BT is the thermal energy, and $\langle g_j|\mathbf{M}|e_i\rangle$ is the dipole-matrix element between each of the different components of the excited (e_i) and ground (g_j) electronic states. The transition energies X_{ij} are computed by numerically diagonalizing the Hamiltonian (3). We point out that the dipole transition from both of the triplet levels, ${}^3T_{1,2}$, that we consider is only partially allowed by SO mixing with the upper-lying singlets, ${}^1T_{1,2}$. This mixing is implicitly considered but for simplicity it is not quantitatively included in the calculation. The emission band shape was obtained by making use of a Monte Carlo integration method.[21] The calculation was performed in the following steps.

(1) Emission occurs from relaxed excited states, i.e., for low temperatures only the bottom of the potential well (surroundings of the minima on APES) is populated. Therefore it was necessary to search for the coordinates $(Q_1^0,Q_2^0,\ldots,Q_6^0)$ of the minima on the multidimensional APES. We looked separately for the minimum of each APES contributing to the emission process. The numerical procedure for finding these minima in the multidimensional space used a generalization of the Newton-Raphson method.[23]

(2) Random values for the six coordinates $(Q_1,Q_2,\ldots,Q_6)$ were generated. Their distribution was a Gaussian, centered around the coordinates of the minima $(Q_1^0,Q_2^0,\ldots,Q_6^0)$. The widths of these Gaussians were $\sigma_\alpha=(k_BT/K_\alpha)^{1/2}$, $\sigma_\epsilon=(k_BT/K_\epsilon)^{1/2}$, and $\sigma_\tau=(k_BT/K_\tau)^{1/2}$, for Q_1, (Q_2,Q_3), and (Q_4,Q_5,Q_6), respectively.

(3) The Hamiltonian (3) was evaluated and diagonalized for each set of generated coordinates $(Q_1,Q_2,\ldots,Q_6)$.

(4) The resulting X_{ij} values were accumulated in 120 energy bins corresponding to the whole range of optical transitions of interest. The procedure was repeated 500 000 times. Additional repetitions did not significantly change the results obtained.

Once data had been collected in this way we took into account the effects of the transition-dipole-matrix element, $\langle g|\mathbf{M}|e\rangle$, and modified each contribution to a particular energy bin (the number of events stored in a particular energy bin). Since the transition dipole moment $\mathbf{M}$ transforms like the Γ_5 irreducible representation[24] of the tetrahedral T_d group, nonzero contributions to the dipole-matrix element would occur only for vectors (or components of vectors) $|e\rangle$ that also transform like Γ_5. After diagonalizing the total Hamiltonian, we performed a Γ_5 projection of each eigenvector so as to obtain the component of the eigenvector that contributes to the emission process. The norm of such a projection gives information about the occupation of the APES contributing to the emission. Finally, the square of the norm of the eigenvector-Γ_5 projection gives the intensity of light emitted within the corresponding energy bin.

III. RESULTS OF NUMERICAL ANALYSIS AND DISCUSSION

For simplicity we started our calculations without consideration of the electron-nuclei coupling to the totally symmetrical vibrational mode α, i.e., we did not include the coordinate Q_1. The effect of this coordinate simply consists of a displacement of the minimum in the Q_1 direction. This produces, apart from a shift of the emission energy, smoother and broader spectra. Therefore this coupling was only included later.

When pure SO coupling is considered, the excited state is split into eight APES's, with various degeneracies, from which only two APES's can contribute to the emission process. Accordingly, the resulting emission spectrum consists of a doublet only. By contrast, when pure JT coupling is considered, only the ${}^3T_2$ level can contribute to the emission process. Coupling between ${}^3T_2$ and ${}^3T_1$ is enabled by the PJT interaction so that two APES's can contribute to the overall emission. But for the lowest temperatures only the bottom of the wells can be populated, so that for the lowest temperatures the emission spectrum would be at most a doublet. Considering both SO and JT interactions leads to a more complicated structure for the lowest excited state, where several APES's can contribute to the overall emission. The tetragonal minima of the lowest excited state are split into four APES's with degeneracies 1, 2, 1, 2 [see Fig. 1(a)] in order of increasing energies. For $\Delta=0$ the degeneracies

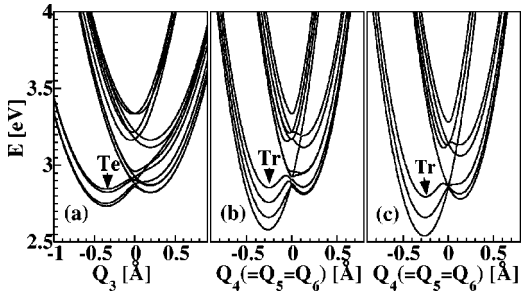

FIG. 1. (a) Cross section along the Q_3 axis ($Q_2=Q_4=Q_5=Q_6=0$) of all APES's on the $^3T_1$ and $^3T_2$ level showing tetragonal minima. Parameters used in the calculation are $\Delta=0.1$ eV, $\lambda=0.07$ eV, $b=1$ eV/Å, $c=0$, $b_{12}=0$, $c_{12}=0$, $K_\epsilon=3$ eV/Å^2, $K_\tau=3$ eV/Å^2. (b) Cross section along the Q_4 axis ($Q_4=Q_5=Q_6$; $Q_2=Q_3=0$) of all APES's on the $^3T_1$ and $^3T_2$ level showing the trigonal minima. Parameters used in the calculation are: $\Delta=0.1$ eV, $\lambda=0.07$ eV, $b=0$, $c=1.2$ eV/Å, $b_{12}=0$, $c_{12}=0$, $K_\epsilon=3$ eV/Å^2, $K_\tau=3$ eV/Å^2. (c) The same as (b) for $\Delta\approx 0$.

become 2, 4. Trigonal minima also split into four APES's with degeneracies 2, 1, 1, 2 [Fig. 1(b)]. The two intermediate APES's become accidentally degenerate for $\Delta=0$ [Fig. 1(c)]. The PJT interaction further modifies the contribution of different APES's to the overall emission and depending on its relation to JT (PJT is greater than JT, or PJT is less than JT) there is a trend to reverse the direction of distortion (from compressed to elongated or vice versa), starting from the highest excited APES's.

If one intends to explain the triplet structure of the emission band shape manifested by tungstates, namely, PWO (see Fig. 2; the details of experiment can be found in Refs. 12,13), the excited-state APES's scheme that seems most likely to result in similar spectral shape is that of Fig. 1(c). Moreover, as mentioned above, it is believed that for tungstates $\Delta\approx 0$. That is why in the following analysis we focused on the situation where $\Delta\approx 0$, the lowest excited state has trigonal minima and the JT interaction is greater than the PJT interaction.

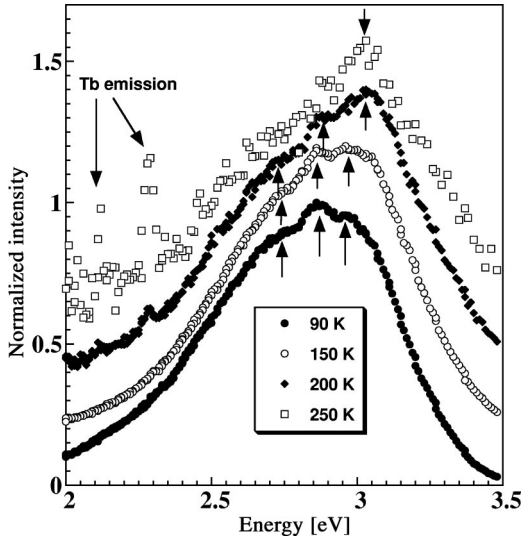

FIG. 2. Normalized x-ray excited emission spectra of PWO:La (460 ppm) measured for temperatures $T=90$ K, 150 K, 200 K, 250 K. Spectra for different temperatures are vertically shifted for better visualization. Triplet structure is marked by arrows. Sharp spectral lines around 2.3 eV and 2.1 eV visible for $T=250$ K (assigned to Tb emission) are due to the emission by unwanted Tb^{3+}, which is present in the raw material for the crystal as an unwanted trace impurity (concentration, several ppm).

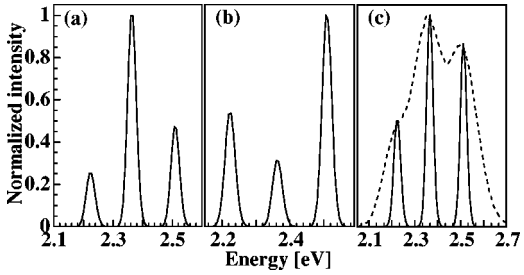

FIG. 3. Normalized emission spectra for the $(^3T_1, ^3T_2)\rightarrow A_1$ transition. Parameters used in the calculation: $\Delta\approx 0$, $\lambda=0.07$ eV, $b=0$, $c=1.2$ eV/Å, $K_\epsilon=3$ eV/Å^2, $K_\tau=3$ eV/Å^2, $W_0=3$ eV. (a) $b_{12}=0$, $c_{12}=0$, $T=4$ K; (b) $b_{12}=0.1$ eV/Å, $c_{12}=0$, $T=4$ K; (c) $b_{12}=0.1$ eV/Å, $c_{12}=0.3$ eV/Å; solid line $T=4$ K, dashed line $T=70$ K.

Under these conditions the calculation following the steps described in the previous section indeed results in an emission band with a triplet structure. For low temperatures at least, this structure is well resolved (Fig. 3). The spectra in Fig. 3 are calculated without considering the spatial separation (shift in Q_i space) of the ground state. Only certain vertical spacing W_0 [see Eq. (6)] of the ground-state and excited-state minima is considered. The separation of the peaks is mainly given by the strength of the SO coupling. The intensities of the peaks are affected by the value of Δ and the strength of PJT coupling (coupling constants b_{12} and c_{12}). When $\Delta\approx 0$ (the case we concentrate on) and PJT coupling is not present, the intensity of the central peak is highly dominant. Switching on PJT coupling by increasing the value of b_{12}, the intensity of the central peak is reduced, even to the point where the high-energy peak becomes dominant. Subsequent increase of c_{12} restores the central-peak intensity [compare Figs. 3(a), 3(b), and 3(c)]. In this way an interplay between PJT coupling constants b_{12} and c_{12} adjusts the intensity relation between the central peak and the peak on the high-energy side of the spectra. Obtaining the same intensity relations for higher values of Δ requires stronger PJT coupling. In agreement with experiment, the structure of the calculated spectra for higher temperatures tends to be less sharp [Fig. 3(c)], but comparing to the experimental band shape, the spectrum is significantly narrower.

The total width of the calculated spectrum is affected by several additional considerations: (1) the position of the ground state, namely, the separation of its minimum in Q_i space with respect to the minima of the excited states—compare Figs. 3(c) and 4(a); (2) the inclusion of the totally symmetrical coordinate Q_1, which not only makes the spectrum broader but also smoother (structure less distinctive)—compare Figs. 4(a) and 4(b); (3) a higher elastic constant corresponding to the ground state with respect to the excited state—compare Figs. 4(b) and 4(c).

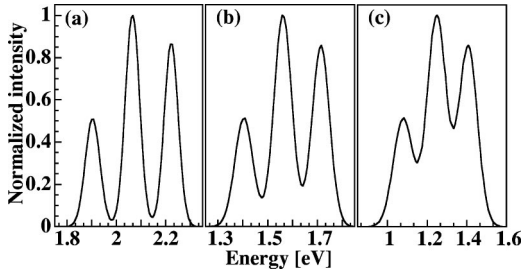

FIG. 4. Normalized emission spectra for the $({}^3T_1, {}^3T_2)\rightarrow A_1$ transition. The calculation is performed by taking into account the spatial separation of the ground state from the excited state (K_g stands for the elastic constant of the ground state) and the totally symmetrical coordinate Q_1. Parameters used in the calculation: $\Delta\approx 0$, $\lambda=0.07$ eV, $b=0$, $c=1.2$ eV/Å, $b_{12}=0.1$ eV/Å, $c_{12}=0.3$ eV/Å, $K_\epsilon=3$ eV/Å^2, $K_\tau=3$ eV/Å^2, $T=4$ K, $W_0=3$ eV. (a) $a=0$; $K_g=3$ eV/Å^2; (b) $a=1$ eV/Å, $K_\alpha=3$ eV/Å^2, $K_g=3$ eV/Å^2; (c) $a=1$ eV/Å, $K_\alpha=3$ eV/Å^2, $K_g=5$ eV/Å^2.

We note that the spectra in Figs. 3 and 4 are calculated with a constant vertical spacing W_0 of the excited-state and ground-state minima. Any change of the coupling parameters changes the energy range of the emission band. In Fig. 5 we chose the vertical spacing W_0 so that for the selected set of parameters the spectral maximum approximately matches the experimental value.

Calculated and measured spectra show similar features, but there are some disagreements that need to be further discussed. As mentioned above, the intensity relations between the central- and high-energy peaks depend on the values of the PJT coupling constants. On the other hand, the intensity of the low-energy peak is given by the origin of the APES (only partially allowed transition) and it is not affected by a change of coupling parameters. The calculated intensity of this peak is significantly lower than the intensity (relative to the central peak) observed in experiment. Nevertheless, a possible increase of the lowest-energy-peak intensity could be expected by including the nonradiative phonon transitions

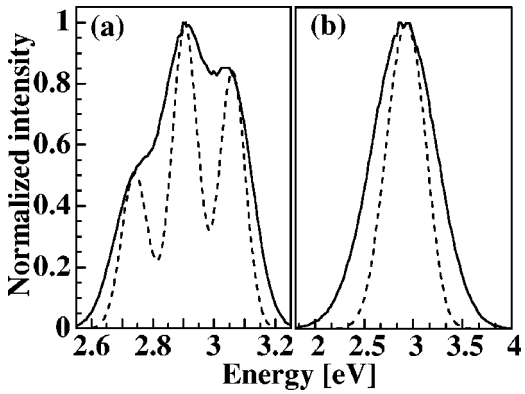

FIG. 5. Normalized emission spectra calculated for the $({}^3T_1, {}^3T_2)\rightarrow A_1$ transition. Parameters used in the calculation: $\Delta\approx 0$, $\lambda=0.07$ eV, $a=1$ eV/Å, $b=0$, $c=1.2$ eV/Å, $b_{12}=0.1$ eV/Å, $c_{12}=0.3$ eV/Å, $K_\alpha=3$ eV/Å^2, $K_\epsilon=3$ eV/Å^2, $K_\tau=3$ eV/Å^2, $K_g=5$ eV/Å^2, $W_0=4.5$ eV; (a) dashed line $T=4$ K, solid line $T=10$ K; (b) dashed line $T=50$ K, solid line $T=200$ K.

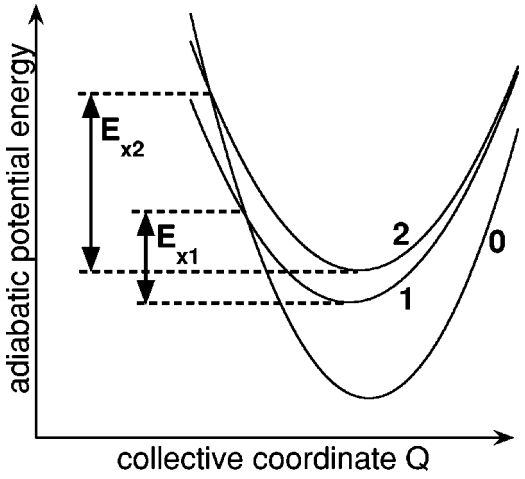

FIG. 6. Energy diagram of the ground state (APES 0) and split excited state (APES's 1,2), showing the energy barriers E_{x1} (E_{x2}) for corresponding nonradiative transitions 1 (2)$\rightarrow$0. The diagram displays the situation in which the energy barrier for the nonradiative transition from the upper APES is higher than that for the lower APES.

from the upper APES's to the lowest one. These transitions would contribute to the population of the lowest APES, thereby increasing the intensity of the emission coming from that APES. Such transitions cannot occur within our scheme where coupling to a bath of lattice phonons is not considered. An extended Hamiltonian with this additional coupling, or alternatively a full quantum-mechanical vibronic calculation, would allow such processes.

According to experimental observation, the intensity of the high-energy peak becomes dominant with increasing temperature (around temperatures higher than 150 K), while for lower temperatures the central peak is dominant. For the calculated spectra though, if the central peak is dominant for low temperatures, it remains dominant for higher temperatures as well (see Fig. 5). This disagreement could be explained by the possible presence of emission quenching to the ground state (not included in the calculation, but observed in experiment[13] for temperatures higher than 150 K). If a quenching barrier for the central APES is lower than the barrier for the highest APES (as sketched in Fig. 6), and simultaneously the transition rate to the ground state is similar or greater, then the quenching from the central APES would be more effective and thus the emission from the highest APES can, at higher temperatures, become dominant.

There is a slight shift of the calculated spectral maximum towards higher energies with increasing temperature. This feature is in accordance with experimental results and physical expectation, even if the shift in experiment is more pronounced. In a quantum-mechanical picture the shift is represented by increased population of the higher vibrational states of the contributing electronic state with increased temperature. Within our semiclassical picture each emission peak is represented by a Gaussian, which is centered around a certain energy. In our case an increase of temperature affects only the width of the Gaussian. This is because for the temperature range considered in our calculation, the potential

wells are deep enough and the part of the well that is involved in the transition is still paraboloidal. Then, the shift of the maximum depends on the intensity of the contributing peaks and the area of their overlap. Therefore a discrepancy between the calculated and measured values is expected.

The experimentally observed emission spectrum in Fig. 2 contains a low-energy tail (not present in the calculated spectrum) that can be a contribution to emission from a source different from the regular $(WO_4)^{2-}$ tungstate group. In Fig. 2 we present the spectrum of La-doped PWO with a concentration of dopant of 460 ppm. Doping by La is used to improve the scintillating properties of PWO but La itself does not contribute to the main blue-emission band that we study. Nevertheless, apart from the dopant, raw material for the crystals almost inevitably contains some trace impurities, like Tb^{3+}, that is responsible for the sharp peaks marked in Fig. 2. The tail on the low-energy side of the spectra is very probably a parasitic emission originating from some other impurity present in the crystal.

The main discrepancy between calculated and observed spectra is in their temperature dependence. As a common feature both types of spectra have a structure that is less sharp with increasing temperature. Nevertheless, calculated spectra tend to lose their structure at relatively low temperatures compared to the experimentally observed temperature dependence. But it should be pointed out that the temperature that enters the calculation within the semiclassical approximation is not the physical temperature. We are working with an effective temperature, which is in fact lower than the real one, and the relatively narrow temperature range in which we observe the structure in the calculated spectra will eventually correspond to a wider physical-temperature interval.

We remark that although in these last paragraphs we have taken pains to point out quantitative defects in the details of our modeling, it should be noted that for the systems under consideration there has heretofore not been even a qualitative explanation for their spectral structure.

IV. CONCLUSION

We showed that a relatively simple semiclassical approach provides the structured emission band of complexes with two closely lying triplet levels. In the present work we focused on PWO crystals and we obtained semiquantitative agreement between the experimental and the calculated spectral shape.

We wish to stress, that the interweaving among different perturbations, such as JT effect, pseudo-JT effect, spin-orbit coupling, and ligand field can play an essential role in determining the complex phenomenology of these systems. The above interweaving, which can be thoroughly studied only using numerical analysis, leads to a four- (or three-) level structure of the lowest excited state. To our knowledge such structure has never been described before for systems with closed-shell $(MO_4)^{q-}$ ions and can be of particular importance in accounting for the experimental data.

ACKNOWLEDGMENTS

This work was supported by the ASCR Grant No. B1010901 and NATO SfP Grant No. 973510. The authors thank L. S. Schulman for many suggestions and stimulating discussions.

[1] G. Blasse, Struct. Bonding (Berlin) **42**, 1 (1980).
[2] C. J. Ballhausen, Theor. Chim. Acta **1**, 285 (1963).
[3] A. L. Spek, A. J. M. Duisenberg, C. J. M. Coremans, and J. H. van der Waals, J. Lumin. **69**, 319 (1996).
[4] Y. D. Glinka, Appl. Phys. Lett. **71**, 566 (1997).
[5] P. Pringsheim, *Fluorescence and Phosporescence* (Interscience, New York, 1949).
[6] F. A. Kroger and J. Bakker, Physica (Amsterdam) **8**, 628 (1941).
[7] W. van Loo, Phys. Status Solidi A **27**, 565 (1979); **28**, 227 (1979).
[8] J. A. Groening and G. Blasse, J. Solid State Chem. **32**, 9 (1980).
[9] CMS Technical Proposal CERN/LHCC **94-38,** LHCC/P1 (1994) (unpublished).
[10] ALICE Technical Proposal CERN/LHCC **95-71,** LHCC/P3 (1995) (unpublished).
[11] M. Nikl, Phys. Status Solidi A **178**, 595 (2000).
[12] K. Polák, M. Nikl, K. Nitsch, M. Kobayashi, M. Ishii, and Y. Usuki, J. Lumin. **72-74**, 781 (1997).
[13] M. Nikl, P. Boháček, E. Mihóková, M. Kobayashi, M. Ishii, Y. Usuki, V. Babin, A. Stolovich, S. Zazubovich, and M. Bacci, J. Lumin. **87-89**, 1136 (2000).
[14] Y. Zhang, N. A. W. Holzwarth, and R. T. Williams, Phys. Rev. B **57**, 12 738 (1998).
[15] M. Bacci, B. D. Bhattacharyya, A. Ranfagni, and G. Viliani, Phys. Lett. **55A**, 489 (1976).
[16] R. Englman, M. Caener, and S. Toaff, J. Phys. Soc. Jpn. **29**, 306 (1970).
[17] Y. Toyozawa and M. Inoue, J. Phys. Soc. Jpn. **9**, 1663 (1966).
[18] Actually, there are two τ_2 vibrational modes that are JT active for a T state in T_d symmetry. Here, for simplicity, only one τ_2 mode is considered.
[19] M. C. M. O'Brien, Phys. Rev. **187**, 407 (1969).
[20] A. Ranfagni, D. Mugnai, M. Bacci, G. Viliani, and M. P. Fontana, Adv. Phys. **32**, 824 (1983).
[21] K. Cho, J. Phys. Soc. Jpn. **25**, 1372 (1968).
[22] C. H. Henry, S. E. Schnatterly, and C. P. Slichter, Phys. Rev. **137A**, 574 (1965).
[23] R. L. Burden and J. D. Faires, *Numerical Analysis* 4th ed. (PWS-KENT, Boston, 1989).
[24] From now on we introduce the Bethe notation for irreducible representations because it is usually adopted for spin-orbit levels.